CONJUNCTIONS AND COLLISION AVOIDANCE WITH ELECTRODYNAMIC TETHERS

Eugene M. Levin
Electrodynamic Technologies, LLC

Abstract

Electrodynamic tethers have very promising applications in debris removal and payload delivery, but require special conjunction analysis methods and collision avoidance strategies. This paper presents results of the analysis of the conjunction geometry and collision probabilities in close approaches between electrodynamic tethers and compact objects, such as satellites, rocket bodies, and debris fragments. Electrodynamic spacecraft do not use fuel and can maneuver constantly. They can "yield" to all cross-traffic and avoid all close approaches with operational spacecraft. Close approaches with debris can be allowed when the collision probabilities are below desired thresholds for each class of objects.

1. Introduction

Electrodynamic propulsion technology is currently in development by NASA, ESA, and JAXA for the purpose of affordable removal of large debris objects from LEO [1, 2]. At the same time, the Naval Research Laboratory is preparing a 3U CubeSat with a 1-km electrodynamic tether for a flight demonstration of electrodynamic propulsion [3]. This type of propulsion does not require fuel. The vehicle is solar powered. The electrodynamic thrust is the Lorentz force acting on the electric current in a long conductor (tether) in the geomagnetic field. Electrons are collected from the ambient plasma on one end and emitted back into the plasma from the other end. The electric current loop is closed through the ionosphere, as demonstrated in the 1993 and 1996 NASA flights with electrodynamic tethers.

To support safe navigation of electrodynamic tethers, proper conjunction analysis and collision avoidance strategies are needed. The typical lengths of electrodynamic tethers for near-term applications are measured in kilometers, and the conjunction geometry is very different from the geometry of conjunctions between compact objects. It is commonly thought that the collision cross-section in a conjunction between a tether and a compact object is represented by the product of the tether length and the size of the object. However, rigorous analysis shows that this is not the case, and that the above assumption leads to grossly overestimated collision probabilities.

Electrodynamic spacecraft do not require fuel and can thrust constantly. Their orbit transfers can take many days, but can result in major orbit changes, including large rotations of the orbital plane, both in the inclination and the node. During these orbit transfers, the electrodynamic spacecraft will cross orbits of numerous tracked objects. However, unlike objects that are incapable of maneuvering and objects that can maneuver only infrequently, the electrodynamic spacecraft can maneuver all the time. They can "yield" to all cross-traffic and avoid all close approaches with operational spacecraft. Close approaches with debris can be allowed when the collision probabilities are below desired thresholds for each class of objects.

There are very few publications analyzing conjunctions with space tethers. Patera [4] showed how to reduce collision probability calculation to a contour integral about the perimeter of the tether hard-body area. Hoyt [5] calculated conjunction frequencies for two tether missions and observed that they are comparable to conjunction frequencies of conventional spacecraft. This paper will focus on conjunction analysis in support of electrodynamic tether missions.

2. Conjunctions with Tethers

Traditionally, it was assumed that electrodynamic tethers will be hanging vertically, stabilized by the gravity gradient. However, it was understood that slowly rotating tethers will perform much better [6]. Thus, they will not be confined to the vicinity of the local vertical and can have any orientation in conjunctions.

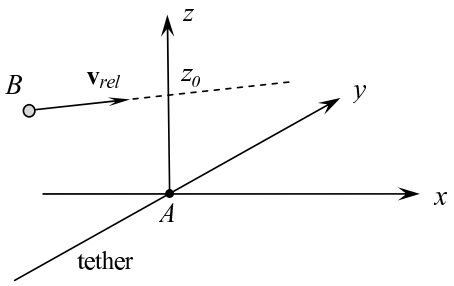

Fig. 1. Conjunction with a rotating tether.

Let us consider an object B passing close to the tether, as shown in Fig. 1. For the purpose of this discussion, we will assume that the object B is a sphere of diameter λ, and that the distance of its closest approach z_0 to the tether line is relatively small compared to the tether length L. We also assume that the curvature of the tether line near the point of the closest approach A is small, and that the relative velocities of rotation of the tether points in the vicinity of point A are small compared to the orbital velocities.

To analyze the conjunction geometry, we introduce a frame of reference $Axyz$, where A is the point of the closest approach on the tether line, the axis Ay is tangent to the tether line at that point, the plane Axy is parallel to the velocity of the object B relative to the point A, and the axis Az is normal to the relative velocity vector $\mathbf{v}_{rel}$, and pointing toward the position of the object B at the time of the closest approach, as illustrated in Fig. 1, so that $z_0 \geqslant 0$.

Let the 3-dimensional probability density of the combined position error at the time of the closest approach be described by the function

$$f = f(x, y, z - z_0). \tag{1}$$

Taking into account that the conjunction is very brief, and the relative motion during the conjunction is nearly linear, the error distribution can be assumed to vary as

$$f = f(x - v_{rx}(t - t_0), y - v_{ry}(t - t_0), z - z_0), \tag{2}$$

where v_{rx} and v_{ry} are the components of the relative velocity vector $\mathbf{v}_{rel}$, and t_0 is the time of the closest approach. We further assume that the standard deviations σ_k associated with the distribution f are large compared to the size λ of the object B, but small compared to the tether length L,

$$\lambda \ll \sigma_k \ll L. \tag{3}$$

Then, the probability of a collision between the object B and the tether can be approximated as

$$P_c \approx \lambda \int_{-\infty}^{\infty} \int_{-\infty}^{\infty} f(x, y, z_0)\, dxdy, \tag{4}$$

because relation (2) implies that the tether "slices" through the distribution (1) at $z = 0$, and collision can only occur in a thin layer

$$|z| \leqslant \lambda/2. \tag{5}$$

In a special case when the distribution (1) can be represented as

$$f = f_1(x, y)\, f_2(z - z_0), \tag{6}$$

we obtain a very simple expression for the collision probability

$$P_c \approx \lambda f_2(z - z_0), \tag{7}$$

or

$$P_c \approx \frac{\lambda}{\sigma_z \sqrt{2\pi}} \exp\left(-\frac{z_0^2}{2\sigma_z^2}\right) \tag{8}$$

for a Gaussian distribution f_2, where σ_z is the standard deviation of the position error in the z-direction. This is applicable, for example, when the tether is oriented horizontally, and the orbits are nearly circular.

One of the major insights provided by formula (8) is that the probability of collision with the tether at a given conjunction does not depend on the tether length and is comparable to the probabilities of collisions between compact objects, such as spacecraft, rocket bodies, and debris. It is somewhat counterintuitive, but keep in mind the difference in the definitions of the closest approach in case of tethers and compact objects. The closest approach between compact objects is measured between their centers of mass, while the closest approach with a tether is measured relative to the tether line and can be far from the center of mass of the tether system.

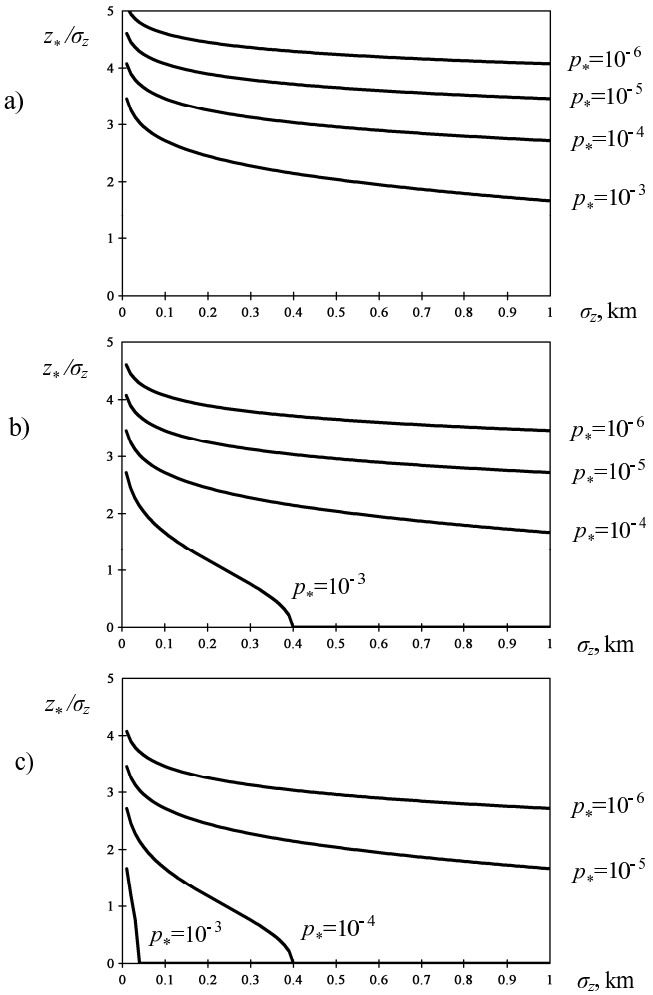

Fig. 2. Threshold approach distances for a) $\lambda = 10$ m, b) $\lambda = 1$ m, c) $\lambda = 0.1$ m.

For the probability of collision to be less than a threshold value p_*, the distance of the closest approach with the tether should exceed a threshold distance z_*,

$$z_0 > z_*. \tag{9}$$

According to (8), the threshold distance is calculated as

$$\frac{z_*}{\sigma_z} = \begin{cases} \sqrt{2\ln(\sigma_*/\sigma_z)}, & \text{with } \sigma_z < \sigma_*, \\ 0, & \text{with } \sigma_z \geqslant \sigma_*, \end{cases} \tag{10}$$

where

$$\sigma_* = \frac{\lambda}{p_* \sqrt{2\pi}}. \tag{11}$$

Fig. 2 plots the ratios z_*/σ_z as functions of σ_z for three typical sizes λ of the object B. Generally, staying 2–3 sigmas away from the tether line should keep the probability of collision low.

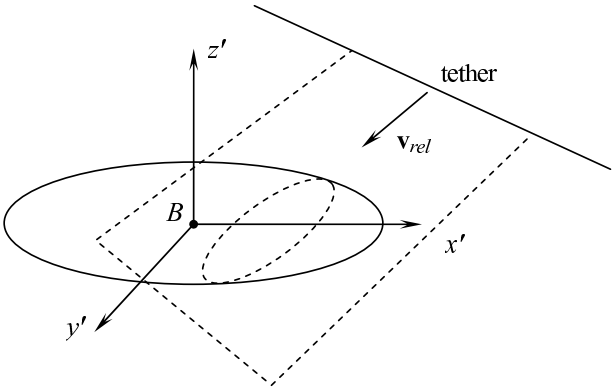

Fig. 3. Motion of the tether trough the position error ellipsoid.

Fig. 3 illustrates the conjunction geometry with respect to a frame of reference associated with the nominal trajectory of the center of mass of the object B. The axes $Bx'y'z'$ can be oriented along the principal axes of the combined position error ellipsoid, if the distribution is Gaussian. The tether moving at a relative velocity $\mathbf{v}_{rel}$ "slices" through the error ellipsoid at some angle. The probability of collision is then calculated similarly to (4) with a 2-dimensional integral taken over the plane of the relative motion of the tether and multiplied by λ.

Let us consider the case when the plane of the relative tether motion depicted in Fig. 3 is parallel to the axis By' and inclined at an angle α to the axis Bx'. We will assume that the combined position error distribution is Gaussian,

$$f = \frac{1}{\sigma_x \sigma_y \sigma_z (2\pi)^{3/2}} \exp\left(-\frac{x'^2}{2\sigma_x^2} - \frac{y'^2}{2\sigma_y^2} - \frac{z'^2}{2\sigma_z^2} \right). \tag{12}$$

We introduce a new coordinate system $B\xi\eta\zeta$ obtained by rotation through the angle α, so that the plane $B\xi\eta$ is parallel to the plane of the relative tether motion, and the axis $B\zeta$ is normal to it, as shown in Fig. 4(a),

$$x' = \xi \cos\alpha - \zeta \sin\alpha, \qquad y' = \eta, \qquad z' = \xi \sin\alpha + \zeta \cos\alpha. \tag{13}$$

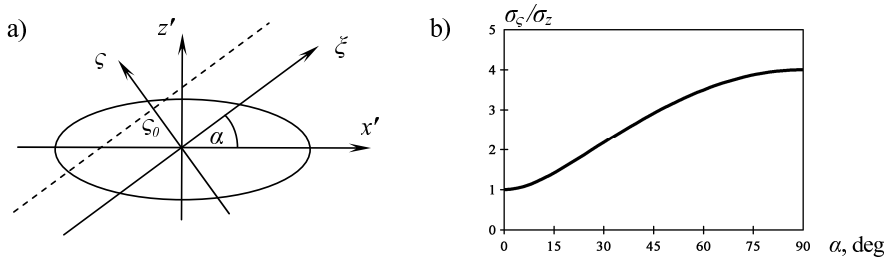

Fig. 4. Parameter σ_ζ as a function of the intersection angle α.

Similar to (4), the probability of collision is calculated as

$$P_c \approx \lambda \int_{-\infty}^{\infty} \int_{-\infty}^{\infty} f \, d\xi d\eta. \tag{14}$$

Substituting (13) into (12) and integrating over ξ and η, we derive

$$P_c \approx \frac{\lambda}{\sigma_\zeta \sqrt{2\pi}} \exp\left(-\frac{\zeta_0^2}{2\sigma_\zeta^2}\right), \tag{15}$$

where ζ_0 is the distance of the closest approach between the center of the object and the tether line, and the parameter σ_ζ is given by

$$\sigma_\zeta = \sqrt{\sigma_x^2 \sin^2\alpha + \sigma_z^2 \cos^2\alpha}. \tag{16}$$

Fig. 4(b) illustrates how σ_ζ depends on the angle α when $\sigma_x/\sigma_z = 4$ (as an example).

Formula (15) generalizes formula (8), and can be generalized further for two-angle rotation. Its meaning is very simple: the probability of collision with the tether is equal in this approximation to the product of the size of the object and the probability density of the distribution of the distance of the closest approach between the object and the tether line with the given orientation of the tether and the direction of the relative velocity.

When the tether orientation is unknown, collision probability calculations are different. First, let us consider the case when the plane of tether rotation is known, but the phase of rotation is unknown. We introduce a frame of reference $Cxyz$ with the origin at the center of mass C of the tether system and the axis Cz normal to the plane of the tether rotation, as shown in Fig. 5.

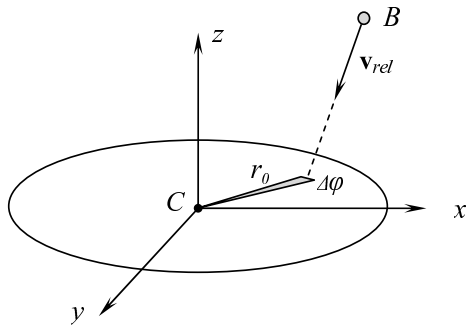

Fig. 5. Conjunction with a known plane and unknown phase of tether rotation.

Let the object B moving at a relative velocity $\mathbf{v}_{rel}$ cross the plane of the tether rotation at a distance r_0 from the center of mass of the tether system. Collision with the tether will occur if the tether is found in the sector $\Delta\varphi \approx \lambda/r_0$ at the time of crossing. If the standard deviations of the combined position error are relatively small compared to the distance r_0, collision probability can be evaluated as

$$P_c = p_1 + p_2, \tag{17}$$

where

$$p_k \approx \begin{cases} \lambda/2\pi r_0, & \text{with } r_0 \leqslant L_k, \\ 0, & \text{with } r_0 > L_k, \end{cases} \tag{18}$$

$k = 1, 2$, and L_1 and L_2 are the distances from the center of mass of the tether system to its end-masses. The phase of the tether rotation is assumed to be distributed uniformly. The probabilities p_1 and p_2 are associated with the two "arms" of the tether system. The difference in the lengths of the arms is especially noticeable with a payload at one end. If the tether system is symmetrical ($L_1 = L_2 = L/2$), we have

$$P_c \approx \begin{cases} \lambda/\pi r_0, & \text{with } r_0 \leqslant L/2, \\ 0, & \text{with } r_0 > L/2. \end{cases} \tag{19}$$

The probability (19) drops much slower with the distance r_0 than the probability (8) with the distance z_0. Even at a respectful distance of $r_0 = 1$ km, the probability of a collision with a 3-m object is relatively

high, on the order of 10^{-3}, compared to the case of a known tether orientation. Thus, it is important to know the tether orientation to estimate the collision probability without exaggeration.

Now, let us consider the case when nothing is known about the tether rotation. Fig. 6 illustrates how the object B enters the sphere of tether rotation and passes at a distance z_0 from the center of mass C of the tether system. The axis Cz is directed to the point of the closest approach, and the axis Cx is aligned with the vector of the relative velocity $\mathbf{v}_{rel}$.

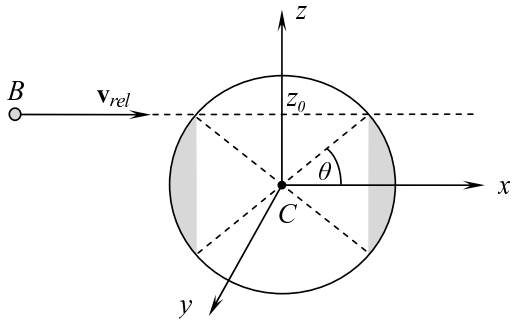

Fig. 6. Conjunction with unknown rotation of the tether.

Again, the collision probabilities are calculated separately for each arm of the tether system. Formula (17) still applies, but with new definitions of p_1 and p_2,

$$p_k \approx \begin{cases} (\lambda/2\pi z_0)\sqrt{1 - z_0^2/L_k^2}, & \text{with } z_0 < L_k, \\ 0, & \text{with } z_0 \geqslant L_k, \end{cases} \tag{20}$$

$k = 1, 2$. These calculations take into account that collision cannot happen when the tether is in the cone encircling the areas shaded gray. The collision sector is defined in the plane Cyz as $\varDelta\varphi \approx \lambda/z_0$. It is assumed that the standard deviations of the combined position error are relatively small compared to the distance z_0.

For a symmetrical tether system ($L_1 = L_2 = L/2$), we have

$$P_c \approx \begin{cases} (\lambda/\pi z_0)\sqrt{1 - 4z_0^2/L^2}, & \text{with } z_0 < L/2, \\ 0, & \text{with } z_0 \geqslant L/2. \end{cases} \tag{21}$$

As it was the case with formula (19), the collision probability (21) drops much slower with the distance of the closest approach compared to the dependency (8) or (15) applicable when the orientation of the tether is known. While approaches at sub-kilometer distances can be acceptable with a known orientation of the tether, such approaches could be perceived as risky when the information about the tether rotation is either limited or unavailable.

3. Conjunction Statistics

Monte-Carlo simulations have shown that conjunctions with operational spacecraft in LEO will be infrequent, weeks apart in typical missions. Being persistently maneuverable and propellantless, electrodynamic vehicles will have no problems avoiding operational spacecraft by very wide margins. Conjunctions with rocket bodies and dead satellites will be more frequent, but still days to weeks apart, and will not present a problem in terms of avoidance either. Most conjunctions will be with debris fragments, numerous, but relatively small.

According to formulas (8), (15), (19), and (21), the probabilities of collision with the tether are proportional to the size λ of the object. At the same time, the trajectories at conjunctions are independent of the size of the object. Thus, we can expect that on average, the cumulative probability of collision in a flux of diverse objects should scale roughly with the cumulative dimension of the objects in the flux

$$\varSigma_D = \sum_{\lambda_k > D} \lambda_k. \tag{22}$$

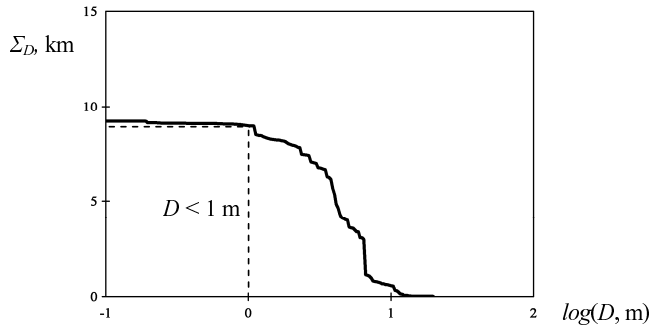

Fig. 7. Cumulative dimension distribution of LEO objects.

Fig. 7 shows the cumulative dimension of the cataloged LEO objects as a function of the threshold size D. The exact dimensions of most debris fragments are not known, and reasonable estimates were used instead. The dashed lines mark the threshold of 1 m. It turns out that the cataloged objects smaller than 1 m add less than 3% to the total amount. Therefore, the long-term cumulative probability of collision with cataloged objects can be reduced by more than 97% on average by just avoiding objects larger than 1 m, but in fact, electrodynamic vehicles are capable of avoiding all tracked objects.

4. Collision Avoidance

Electrodynamic vehicles can thrust constantly and do not stay in fixed orbits. Once a high level orbit transfer plan for a given vehicle is formulated, we choose a reasonable planning horizon for daily operations. While the entire mission could last many days, the operational prediction interval could be much shorter, on the order of one day. We then define a likely maneuvering zone as a tube around the reference trajectory extended over the chosen prediction period and study the traffic of cataloged objects crossing the maneuvering zone at times when the electrodynamic vehicle is expected to be within a certain "alert distance." For example, the tube could be 20–30 km in diameter, and the alert distance could be 40–60 km or more. These values could vary with time to reflect the growth of the prediction uncertainties.

It is convenient in some respects to introduce the arclength s measured along the reference trajectory of the center of mass of the electrodynamic vehicle. For each point s, there will be a moment t when the vehicle is supposed to arrive at this point. Geometrically, the cross-traffic events can be characterized by the arclength s_k of the point of the closest approach to the reference trajectory, the time t_k when it occurs, the range r_k and the out-of-plane angle ϑ_k at which it occurs, the velocity of the objects v_k at that moment, and the angle α_k between the trajectories at the crossing point.

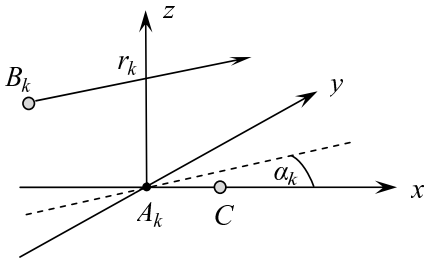

Fig. 8. Conjunctions along the nominal flight path.

Let us consider a conjunction event when an object B_k crosses the path with the electrodynamic vehicle. We will assume that the motion is linear during the event and introduce a reference frame A_kxyz, where the axis A_kx is aligned with the geocentric velocity vector $\mathbf{v}_C$ of the center of mass C of the tether system, the plane A_kxy is parallel to the geocentric velocity vector $\mathbf{v}_k$ of the object B_k, the axis A_kz is normal to both velocity vectors, and point A_k is the point of the closest approach between the two trajectories.

It is generally different from the closest approach between the points B and C because of its timing. For conjunctions in LEO, the axis A_kz will typically be pointing within a few degrees from the local vertical, because most orbits have low eccentricities. Even in conjunctions with GTO objects, the angle between the axis A_kz and the local vertical will be relatively small, because these conjunctions will take place near the perigee of the GTO orbit.

The motion of the object B_k with respect to the axes A_kxyz can be described as

$$x = v_k \Delta t \cos\alpha_k, \quad y = v_k \Delta t \sin\alpha_k, \quad z = r_k, \tag{23}$$

where $v_k = |\mathbf{v}_k|$ is the velocity of the object B_k, α_k is the angle between the velocity vector $\mathbf{v}_k$ and the axis A_kx, $\Delta t = t - t_k$ is the time elapsed from the moment t_k of the closest approach between the trajectories, and r_k is the distance of the closest approach.

Each point of the reference trajectory of the center of mass of the electrodynamic vehicle corresponds to a certain value of the arclength s. In the conjunction area, we have $x = \Delta s$ with high degree of accuracy, where $\Delta s = s - s_k$, and s_k is the arclength corresponding to the point A_k. Then, for any given threshold distance $D_k \geqslant r_k$, the points $s = s_k + \Delta s$ of the reference trajectory that satisfy the following condition

$$(\Delta s - v_k \Delta t \cos\alpha_k)^2 + (v_k \Delta t \sin\alpha_k)^2 + r_k^2 \leqslant D_k^2 \tag{24}$$

will be within the range D_k from the object B_k at the time $t = t_k + \Delta t$. We will call it a "stay-away zone" created by this conjunction along the nominal path of the electrodynamic vehicle.

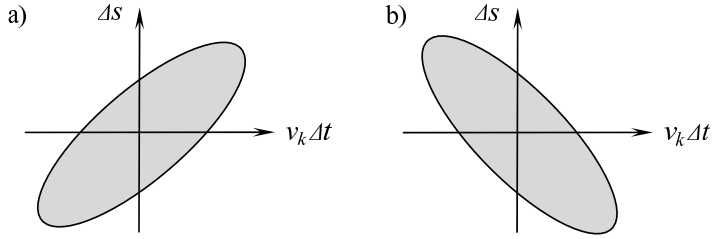

Fig. 9. The shape of the stay-away zones: a) $\cos\alpha_k > 0$, b) $\cos\alpha_k < 0$.

Condition (24) is easily resolved with respect to Δs, but it also has a very simple geometric interpretation. After the following substitution

$$v_k \Delta t = (\xi - \eta)/\sqrt{2}, \qquad \Delta s = (\xi + \eta)/\sqrt{2}, \tag{25}$$

we arrive at

$$\xi^2(1 - \cos\alpha_k) + \eta^2(1 + \cos\alpha_k) \leqslant D_k^2 - r_k^2. \tag{26}$$

Drawn on the plain $(v_k \Delta t, \Delta s)$, these areas are constrained by ellipses whose primary axes are oriented at 45° with respect to the axes $v_k \Delta t$ and Δs, as shown in Fig. 9.

Fig. 10 shows sample stay-away zones from simulations with a threshold distance of $D_k = 10$ km. The bold lines going from the lower left to the upper right corners of the charts represent the reference trajectories of the electrodynamic vehicle. Arrows in the charts show how the electrodynamic vehicle can avoid many stay-away zones completely by a small adjustment of the timing of its arrival to the conjunction area. However, in case of nearly head-on conjunctions, such as shown in Fig. 11(a), when $\cos\alpha_k$ is close to -1, the required adjustment may not be small.

In this case, we can increase the distance of the closest approach between the trajectories by a certain amount Δr to reduce the projection of the stay-away zone onto the path of the electrodynamic vehicle. This as achieved by arriving at the conjunction at slightly different altitude, because the axis A_kz is close to the local vertical for LEO orbits, as noted earlier. We thus extend the notion of the stay-away zone into the 3-dimensional parameter space $(v_k \Delta t, \Delta s, \Delta r)$, where the stay-away zones are bounded by ellipsoids,

$$(\Delta s - v_k \Delta t \cos\alpha_k)^2 + (v_k \Delta t \sin\alpha_k)^2 + (\Delta r + r_k)^2 \leqslant D_k^2. \tag{27}$$

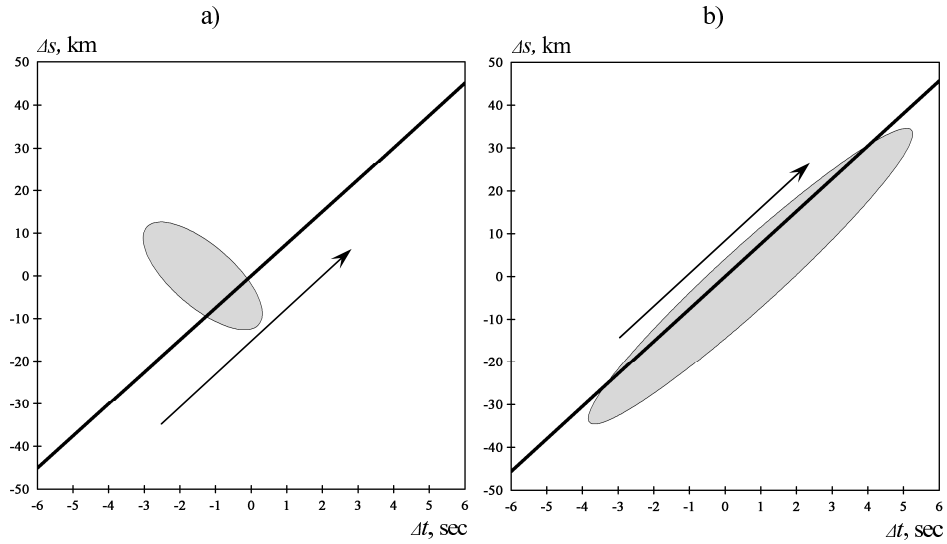

Fig. 10. Stay-away zones along the nominal flight path.

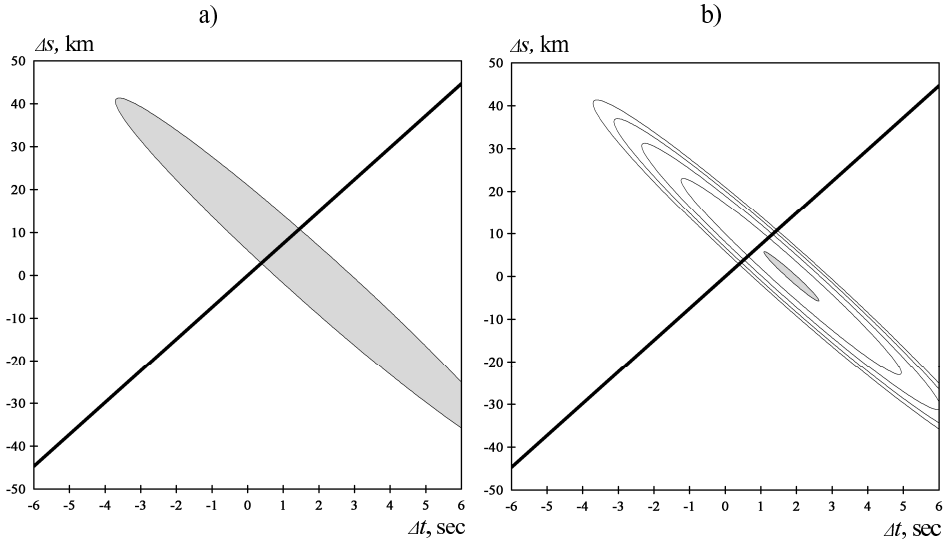

Fig. 11. Avoiding a head-on conjunction (a) by altitude variation (b).

Fig. 11 illustrates how a few kilometers in altitude change can reduce the projection of a stay-away zone created by a nearly head-on conjunction to a small area off the path of the electrodynamic vehicle. Here, the altitude difference between the consequent nested ellipses is 1 km.

The stay-away zones can be very different for different LEO objects. Sizable stay-away zones could be assigned to high-value assets, while conjunctions with debris fragments can be handled by using fairly small stay-away zones. Operational satellites should generally be passed at ranges larger than the distance from the center of mass of the tether system to its farthest end-mass, while debris fragments can be allowed to penetrate the sphere of the tether reach when the phase of the tether rotation is adjusted to provide sufficient miss distances. Thus, the stay-away zones should be used more like references for charting the safest path of the electrodynamic vehicle.

It is convenient to think about adjusting the flight plans in a 3-dimensional space of time t, the arclength s along the reference trajectory, and the elevation $\triangle R$ above or below the reference trajectory. This notion is illustrated in Fig. 12, where the dashed line represents the nominal flight plan. As discussed earlier, the stay-away zones appear in this space as ellipsoids (in a certain approximation). Adjustments to the original flight plan should aim at either by-passing the stay-away zones entirely, or possibly flying through some of

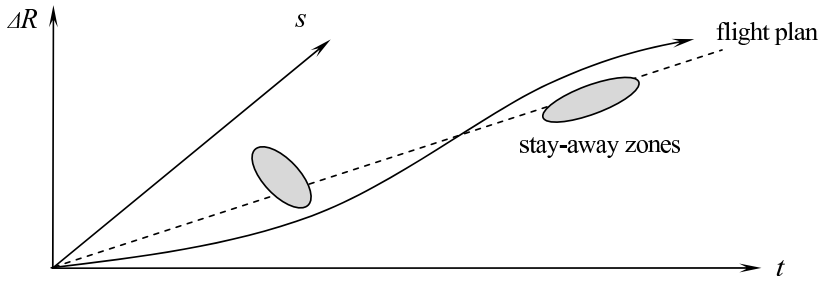

Fig. 12. Adjusting the flight plan to avoid stay-away zones.

them at their periphery, if that conjunction is with a debris fragment.

Raising or lowering the average altitude for a limited period of time can be used to shift the time of arrival at a conjunction and to increase the radial miss distance as well. The rates of altitude change for electrodynamic vehicles can exceed 10 km/hour. Even at a fraction of this rate, these maneuvers can result in along-track shifts of tens of kilometers in one orbit and much more over longer periods of time. The radial miss distance can be also sufficiently increased by slight changes in the eccentricity. Other control options include slight changes in the orbit inclination and phasing the tether rotation to increase the miss distances. Keeping in mind that electrodynamic vehicles cannot run out of fuel, this gives them enough maneuvering capacity to avoid all close approaches on their way.

5. Conclusions

With proper flight planning and execution, collision risks associated with electrodynamic vehicles can be less than with conventional spacecraft, even though the tether length can be measured in kilometers. These vehicles can avoid close approaches with operational and defunct spacecraft and rocket bodies by wide margins, while minimizing the risks to the elements of the vehicle itself at conjunctions with tracked debris fragments. Being propellantless, they never run out of fuel and can continue collision avoidance throughout their missions.

Acknowledgment

This analysis was performed within the framework of the NASA Clean Space Project.

References

1. Levin, E., Pearson, J., and Carroll, J., Wholesale Debris Removal From LEO, Acta Astronautica, v.73, April-May 2012, pp.100-108, http://electrodynamictechnologies.com/PDF/ActaAstr-2012.pdf.

2. Pearson, J., Levin, E., and Carroll, J., Affordable Debris Removal and Collection in LEO, Paper IAC-12-A6.6.7, 63rd International Astronautical Congress, Naples, Italy, October 1-5, 2012.

3. Coffey, S., Kelm, B., Hoskins, A., Carroll, J., and Levin, E., Tethered Electrodynamic Propulsion CubeSat Experiment, Air Force Orbital Resources Ionosphere Conference, Dayton, Ohio, January 12-14, 2010.

4. Patera, R.L., Method for Calculating Collision Probability Between a Satellite and a Space Tether, J. of Guidance, Control, and Dynamics, Vol. 25, No. 5, 2002, pp. 940-945.

5. Hoyt, R. and Buller, J., Analysis of the Interaction of Space Tethers with Catalogued Space Objects, AIAA Paper 05-4430, 2005.

6. Levin, E.M., Dynamic Analysis of Space Tether Missions, Advances in the Astronautical Sciences, Vol. 126, 2007, 454 pp.